

# Graphene-Based Linear Tandem Micro-Supercapacitors with Metal-Free Current Collectors and High-Voltage Output

Xiaoyu Shi, Zhong-Shuai Wu,\* Jieqiong Qin, Shuanghao Zheng, Sen Wang, Feng Zhou, Chenglin Sun, and Xinhe Bao

Printable supercapacitors are regarded as a promising class of microscale power source, but are facing challenges derived from conventional sandwich-like geometry. Herein, the printable fabrication of new-type planar graphene-based linear tandem micro-supercapacitors (LTMSs) on diverse substrates with symmetric and asymmetric configuration, high-voltage output, tailored capacitance, and outstanding flexibility is demonstrated. The resulting graphene-based LTMSs consisting of 10 micro-supercapacitors (MSs) present efficient high-voltage output of 8.0 V, suggestive of superior uniformity of the entire integrated device. Meanwhile, LTMSs possess remarkable flexibility without obvious capacitance degradation under different bending states. Moreover, areal capacitance of LTMSs can be sufficiently modulated by incorporating polyaniline-based pseudocapacitive nanosheets into graphene electrodes, showing enhanced capacitance of  $7.6 \text{ mF cm}^{-2}$ . To further improve the voltage output and energy density, asymmetric LTMSs are fabricated through controlled printing of linear-patterned graphene as negative electrodes and  $\text{MnO}_2$  nanosheets as positive electrodes. Notably, the asymmetric LTMSs from three serially connected MSs are easily extended to 5.4 V, triple voltage output of the single cell (1.8 V), suggestive of the versatile applicability of this technique. Therefore, this work offers numerous opportunities of graphene and analogous nanosheets for one-step scalable fabrication of flexible tandem energy storage devices integrating with printed electronics on same substrate.

The rapid development of emerging printed electronics with outstanding flexibility, thinness, miniaturization, and smart functionalities has significantly accelerated the innovation of next-generation printed energy storage devices with matchable features in different dimensionalities.<sup>[1–6]</sup> Printable supercapacitors,<sup>[7–10]</sup> based on printed films on plastic or paper substrates, have been considerably regarded as a promising class of compact, lightweight, and reliable energy storage devices, which are specifically desired to efficiently integrate for printed electronics, e.g., photovoltaics, piezoelectrics, sensors and other circuits.<sup>[11]</sup> Despite of enormous advancements in nanostructured electrode materials (e.g., carbon nanotube,<sup>[7]</sup> activated carbon,<sup>[12]</sup> graphene,<sup>[10,13]</sup> cobalt hydroxide,<sup>[14]</sup>  $\text{Fe}_3\text{O}_4$ ,<sup>[15]</sup> carbon nanotube/ $\text{RuO}_2$ ,<sup>[16]</sup> and graphene/polyaniline<sup>[17]</sup>), solid-state electrolytes and separators (such as polymer,<sup>[18]</sup> graphene oxide,<sup>[10]</sup> and inorganic ceramics<sup>[19]</sup>), and scalable manufacturing technologies (e.g., inkjet printing,<sup>[16,20]</sup> screen printing,<sup>[17]</sup> spray coating,<sup>[7,15]</sup> roll-to-roll printing,<sup>[21]</sup> and 3D printing<sup>[22]</sup>), printable supercapacitors

are still facing huge challenges arising from the stacked device geometry in sandwich-like structure.<sup>[10]</sup> First, the separator and electrolyte are usually used, resulting in poor interfaces of the different components and integrity of supercapacitors particularly under bending states.<sup>[10]</sup> Second, utilizing two substrates substantially increases the cell volume and mass, eventually reducing the volumetric and gravimetric capacitances.<sup>[23]</sup> Third, additional metal interconnects are often required when multiple, separated supercapacitors are connected in series and/or parallel for boosting the output of voltage and/or capacitance, which is a big bottleneck for integrating printable supercapacitors with designable printed electronics on one same substrate.<sup>[24]</sup>

To overcome these obstacles, considerable efforts have been devoted to developing planar micro-supercapacitors (MSs) consisting of coplanar interdigital electrodes on single substrate.<sup>[25–31]</sup> In this planar geometry, a narrow empty interspace between cathode and anode is presented as separator

X. Y. Shi, Prof. Z.-S. Wu, J. Q. Qin, S. H. Zheng, S. Wang,  
Dr. F. Zhou, Prof. C. L. Sun, Prof. X. H. Bao  
Dalian National Laboratory for Clean Energy  
Dalian Institute of Chemical Physics  
Chinese Academy of Sciences  
457 Zhongshan Road, Dalian 116023, China  
E-mail: wuzs@dicp.ac.cn

X. Y. Shi  
Department of Chemical Physics  
University of Science and Technology of China  
96 JinZhai Road, Hefei 230026, P. R. China

X. Y. Shi, S. H. Zheng, Prof. X. H. Bao  
State Key Laboratory of Catalysis  
Dalian Institute of Chemical Physics  
Chinese Academy of Sciences  
457 Zhongshan Road, Dalian 116023, China

J. Q. Qin, S. H. Zheng, S. Wang  
University of Chinese Academy of Sciences  
19 A Yuquan Rd, Shijingshan District, Beijing 100049, China

DOI: 10.1002/adma.201703034

to prevent electrical short circuit, enabling good electrode–electrolyte interfaces and mechanical flexibility by maximally eliminating the possibility of multilayer delamination in stacked supercapacitors, and seamless integration of printed electronics on single substrate.<sup>[25,32–34]</sup> Recently, 2D materials, such as graphene<sup>[33,35–40]</sup> and analogous nanosheets (e.g., MXene,<sup>[41–43]</sup> VS<sub>2</sub>,<sup>[44]</sup> thiophene,<sup>[45]</sup> polypyrrole,<sup>[46]</sup> and polyaniline<sup>[47]</sup>) are becoming a highly potential class of high-performance material platform for constructing planar MSs, in which they can efficiently utilize their intriguing features, like 2D thinness and high surface area, for on-chip energy storage.<sup>[48]</sup> Despite great progress of 2D nanosheets for MSs, the designed construction of structurally defined planar MSs with exceptional flexibility and integration in form factors on one substrate has not been fully exploited.

Herein, we demonstrate a universal protocol for printable fabrication of graphene-based linear tandem MSs (denoted as LTMSs) on diverse substrates, with symmetric and asymmetric configurations, high-voltage output, tailored capacitance and outstanding flexibility. The novel all-solid-state planar LTMSs are manufactured based on fully printed graphene-based materials on the flexible substrates (e.g., A4 paper and nylon membrane) with assistance of inconsecutively parallel linear mask, in which the deposition and patterning of the film electrodes as well as metal-free current collectors and interconnects are achieved in a single step, allowing for simplified production for serially connected integrated circuits, without requirement of additional metal-based current collectors and interconnects. Using this strategy, LTMSs in both symmetric and asymmetric configurations can be readily produced on the targeted substrates from one or two kinds of 2D graphene (e.g., electrochemically exfoliated graphene (EG)) and pseudocapacitive nanosheets (e.g., mesoporous polyaniline-graphene (PANI-G) and MnO<sub>2</sub>). As a proof of the concept, graphene-based LTMSs consisting of ten tandem MSs, with areal capacitance of 4.9 mF cm<sup>-2</sup>, presented efficient high-voltage output of 8.0 V, demonstrative of superior uniformity of the entire integrated device. Further, the resulting LTMSs underscored excellent flexibility, and very stable performance without obvious capacitance degradation under different bending states. Moreover, areal capacitance of LTMSs can be sufficiently modulated by incorporating high-capacitance pseudocapacitive PANI-G nanosheets into patterned electrodes of single MSs, showing enhanced capacitance of 7.6 mF cm<sup>-2</sup>. Moreover, our approach also provided a new platform for fabricating asymmetric LTMSs to simultaneously improve the voltage and energy density, by controllably printing linear-patterned EG films as negative electrodes and MnO<sub>2</sub> films as positive electrodes, respectively. Notably, the asymmetric LTMSs from three serially connected MSs were easily extended to 5.4 V, triple voltage output of the single cell (1.8 V), suggestive of the versatile applicability of our technique. Therefore, this work offers the impressive opportunities for one-step scalable fabrication of flexible tandem energy storage devices integrating with printed electronics on same substrate.

**Figure 1** depicts the representative schematic of fabricating LTMSs (denoted as GP-LTMSs) on A4 paper based on the printable film (GP) of EG nanosheets and electrochemically active yet conducting PH1000. To engineer the GP-LTMSs, we

first produced high-quality EG nanosheets, with lateral size of 3–10 μm and layer number of ≤3 (Figure 1c–e; Figure S1, Supporting Information), as described previously.<sup>[49,50]</sup> Second, the conducting hybrid ink of EG (0.6 mg mL<sup>-1</sup>) and PH1000 (10 mg mL<sup>-1</sup>) was prepared in isopropanol (IPA) by sonication for 30 min (see details in the Experimental Section). Notably, the introduction of PH1000 is very helpful for the formation of highly conductive and continuous film since PH1000 was strongly adhered to the surface of EG (Figure S2, Supporting Information).<sup>[13]</sup> By spray-coating GP hybrid ink through an inconsecutively parallel linear customized mask, the linear arrays of patterned film electrodes were readily realized in a single step on A4 paper (Figure 1a). It is pointed out that, to demonstrate our concept of LTMSs, we chose the large interspace gaps of 0.1 cm between two adjacent electrode fingers to avoid short circuit for the facile fabrication of LTMSs. The digital image of GP-LTMSs consisting of ten tandem MSs is shown in Figure 1b. Top-view scanning electron microscopy (SEM) image of the printed GP patterns on A4 paper (Figure 1f) reveals large-area uniformity and excellent interfacial adherence (Figure S3a,b, Supporting Information) to the deposited paper. As expected, the resulting GP hybrid film exhibited a lower resistance and higher conductivity than pure EG film (Figure S4, Supporting Information). Subsequently, a polymer gel electrolyte of H<sub>2</sub>SO<sub>4</sub>/polyvinyl alcohol (H<sub>2</sub>SO<sub>4</sub>/PVA), serving as solid-state electrolyte, was carefully drop-casted onto the localized electrode area of two parallel linear electrodes, and solidified for 12 h. It should be emphasized that the single linear patterns positioned between the adjacent double parallel linear electrodes were utilized as electrical interconnects, as indicated in Figure 1a. In this case, although the overall electrode length of LTMSs is increased, the ionic diffusion length of LTMSs is actually kept the same as the length of each single GP-MSs because the gel electrolyte is well localized and limited in the parallel electrode patterns and separated by the single interconnects. Finally, all-solid-state paper-based GP-LTMSs integrating ten serially connected MSs were readily constructed. Importantly, this printing technique is highly flexible for scalable fabrication of GP-LTMSs, without the addition of polymer binder, additive, liquid-electrolyte, separator, metal-based current collectors, and wire interconnects, capable of tailored device configurations, electrode size, and multiple functionalities.

To demonstrate the outstanding performance of GP-LTMSs, we first examined the single cell of MSs (GP-MSs) based on GP film arrays (2 mL ink) through the optimization of the length and width of microelectrodes (Figures S5 and S6, Supporting Information), using H<sub>2</sub>SO<sub>4</sub>/PVA gel electrolyte (**Figure 2**). Then, electrochemical performance of GP-MSs was thus measured by cyclic voltammetry (CV) curves at scan rates from 2 to 500 mV s<sup>-1</sup> (Figure 2a,b) and galvanostatic charge–discharge (GCD) profiles at different current densities of 0.1–1 mA cm<sup>-2</sup> (Figure 2d). Notably, GP-MSs presented nearly rectangular CV shape, and GCD curves presented highly symmetric triangle shape, indicative of typical electrical double-layer capacitive behavior. Furthermore, it was calculated that areal capacitance of GP-MSs recorded at 2 mV s<sup>-1</sup> was 4.9 mF cm<sup>-2</sup> (Figure 2c), which was much higher than those of recently reported carbon-based MSs, such as 0.08 mF cm<sup>-2</sup> for methane plasma rGO,<sup>[35]</sup> 3.93 mF cm<sup>-2</sup> for graphene/carbon nanotube carpets,<sup>[51]</sup>

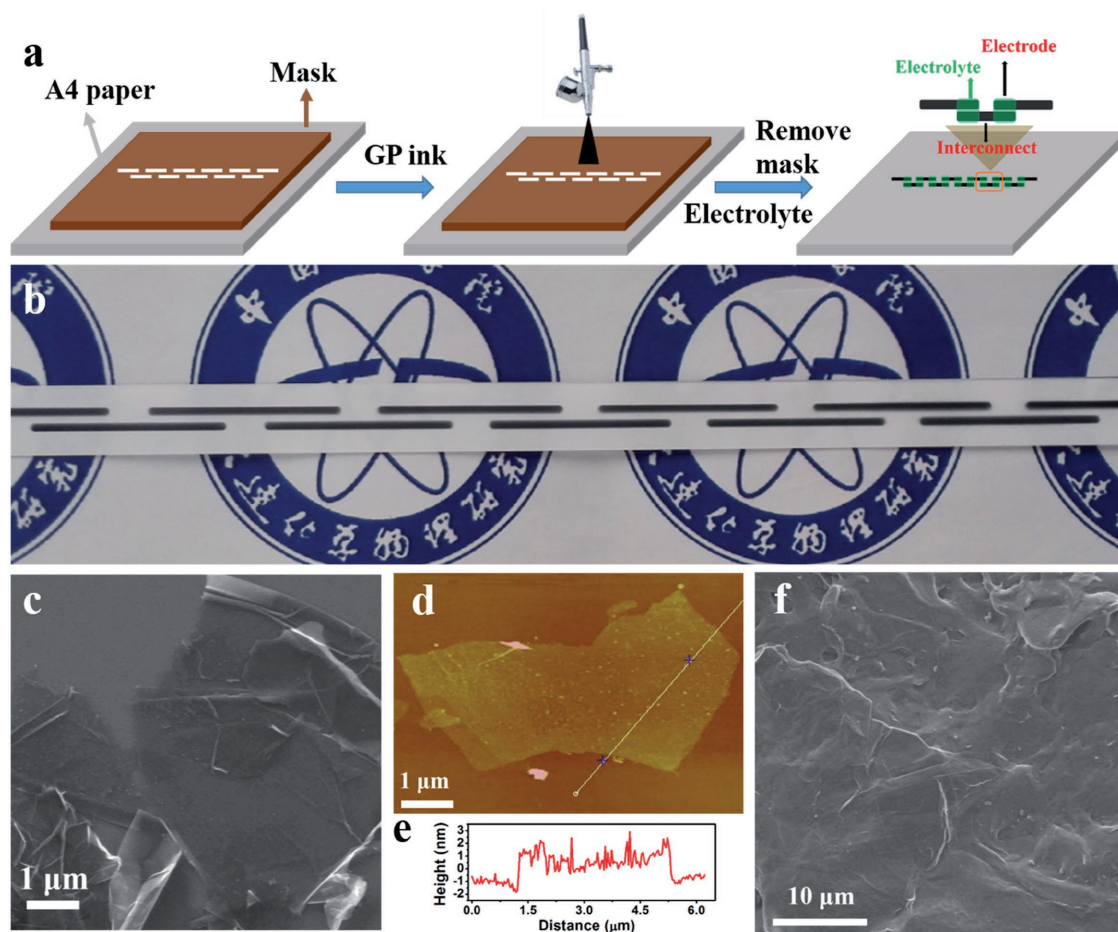


**Figure 1.** Fabrication and characterization of GP-LTMSs. a) Schematic of the fabrication of GP-LTMSs. b) Photograph of paper-based GP-LTMSs consisting of ten serially connected GP-MSs. c) SEM image of EG on Si wafer. d) Atomic force microscopy (AFM) image and e) height profile of EG. f) Top-view SEM image of GP-LTMSs.

0.28  $\text{mF cm}^{-2}$  for electrochemically rGO,<sup>[52]</sup> 0.51  $\text{mF cm}^{-2}$  for laser written GO film,<sup>[32]</sup> and 2.1  $\text{mF cm}^{-2}$  for activated carbon.<sup>[53]</sup> It is noted that GP-MSs disclosed outstanding rate performance. A high capacitance of 3.16  $\text{mF cm}^{-2}$ , about 64.6% of the value at 2  $\text{mV s}^{-1}$ , was maintained even at a high scan rate of 500  $\text{mV s}^{-1}$ , which is attributed to high conductivity of GP film (Figure S4, Supporting Information). Meanwhile, our GP-MSs showed outstanding cycling stability, with 91.1% capacitance retention after 10 000 cycles (Figure 2e). It should be mentioned that, with the increase of the length or width of electrodes, the individual GP-MSs would result in the negative effects on the electrochemical performance, e.g., decreased rate capability (Figures S5 and S6, Supporting Information), due to the longer ionic transfer pathway of the longer or wider linear electrodes. Moreover, electrochemical performance of GP-MSs was readily modulated by varying volume of ink used for GP film patterns (Figure 2f; Figure S7, Supporting Information). However, it was worth noting that, when the ink volume increased from 0.5 to 2 mL, the corresponding equivalent series resistance (ESR) of GP-MSs declined sharply from 910 to 180  $\Omega$  while ESR increased to 360  $\Omega$  using 2.5 mL ink, indicating that a suitable ink volume is required for the formation of continuous film for GP-MSs. In addition, the usage of metal-based

current collector (Au), selection of aqueous electrolyte, and optimization of the ratio of PH1000 and EG also significantly influence the ESR of GP-MSs (Figure S8, Supporting Information).

To validate the exceptional integration of GP-LTMSs, we constructed long-ribbon-like GP-LTMSs consisting of ten serially connected GP-MSs, based on the fully printed GP linear patterns (Figure 3a). The CV curves of GP-LTMSs from 1 to 10 GP-MSs in series displayed a nearly identical rectangular shape tested at 100  $\text{mV s}^{-1}$  (Figure 3c). As a result, GP-LTMSs showed a step-wise linear increase in the working voltage from 0.8 to 8.0 V by increasing the number of serial cells, while the corresponding current and capacitance monotonically decreased (Figure 3c,d), indicative of excellent performance uniformity. Moreover, this result is well supported by GCD profiles of GP-LTMSs connected 5 and 10 GP-MSs in series, which showed a symmetric shape at a current density of 0.05  $\text{mA cm}^{-2}$ . Correspondingly, the integrated voltage increased to five (4.0 V) and ten times (8.0 V) in comparison with single GP-MSs (0.8 V), while the charge and discharge time almost kept invariable (Figure 3e). It is pointed out that although the overall capacitance of our LTMSs was nearly inversely proportional to the device number and their ESR roughly changed linearly with the device number (Figure 3d; Figure S9, Supporting Information), the slight

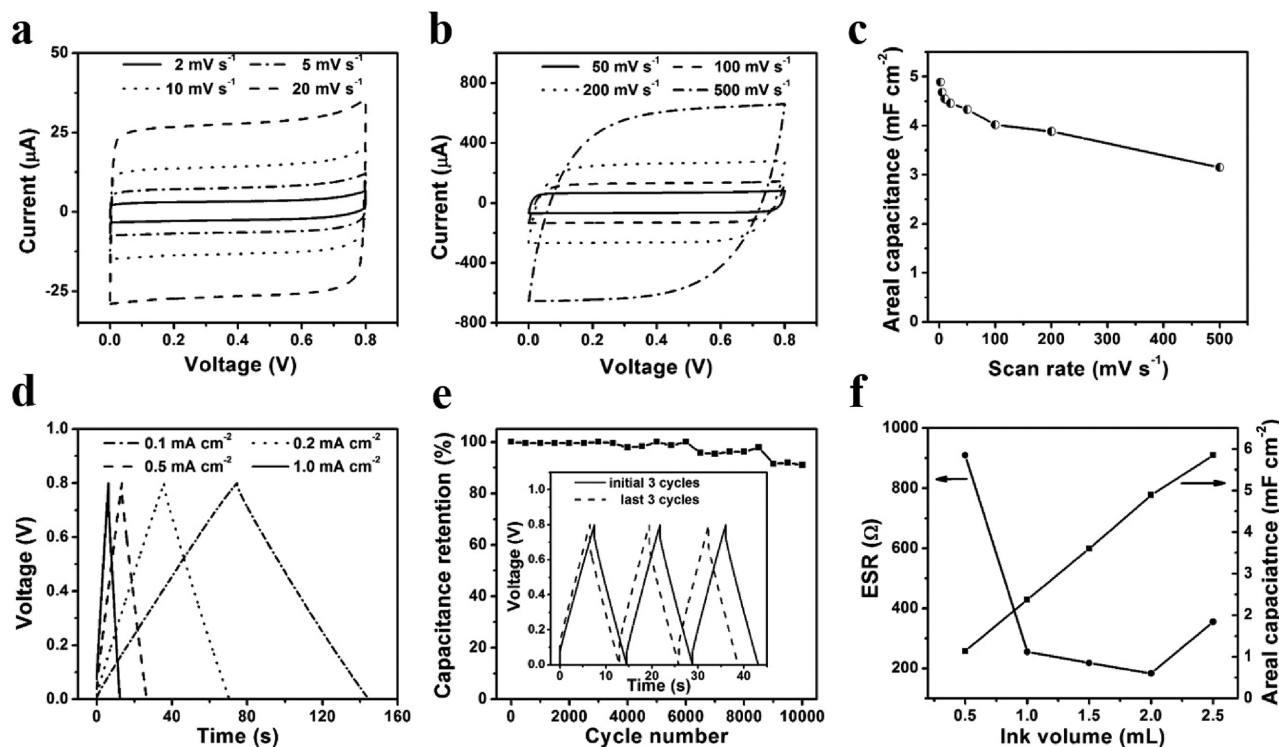


**Figure 2.** Electrochemical characterization of single GP-MSs. a,b) CV curves of GP-MSs using  $\text{H}_2\text{SO}_4/\text{PVA}$  electrolyte, measured at different scan rates from 2 to  $500 \text{ mV s}^{-1}$ . c) Areal capacitance of GP-MSs as a function of scan rate. d) GCD profiles of GP-MSs tested at different current densities. e) Cycling stability of GP-MSs for 10 000 cycles. Inset: GCD curves of GP-MSs of initial and last three cycles. f) Areal capacitance obtained at  $2 \text{ mV s}^{-1}$  and ESR of GP-MSs as functions of spray-coated ink volume.

performance deterioration from the parallel comparison of the experimental overall capacitance and ESR with the theoretical values of LTMSs was still observed (Tables S1 and S2, Supporting Information), mainly caused by the relatively limited electrical conductivity ( $200 \text{ S cm}^{-1}$ ) of interconnects of GP materials. This will become more obvious when the length is further extended. Therefore, to further improve the performance disparity, highly conductive interconnects (such as Cu, Ag) among individual MSs are required. Remarkably, our integrated GP-LTMSs underscored outstanding mechanical flexibility and performance stability. When paper-based GP-LTMSs serially connected 10 GP-MSs were bended in different states ( $L/L_0$ , whereas  $L$  represents the distance between two endpoints of GP-LTMSs in different bent states, and  $L_0$  is the total flat length of 14.5 cm), CV curves obtained at  $200 \text{ mV s}^{-1}$  in different bending states uncovered the slight capacitance degradation, only 6% loss of initial capacitance under a high bent state ( $L/L_0 = 40\%$ ). Moreover, neither structural instability nor delamination of the GP film on paper substrate was observed even after highly bending. Besides, the GP-MSs connected in parallel also demonstrated the outstanding integration and performance uniformity (Figure S11, Supporting Information). These results further highlight the enormous applicability of our unitized power source for wearable electronics, e.g., smart watches.

To further demonstrate wide applicability and significantly enhance the capacitance of linear tandem devices, we also adopted the same manufacturing procedure for fabricating

LTMSs (GP/PANI-G/GP-LTMSs) based on alternating deposited hybrid film of GP and PANI-G nanosheets,<sup>[47]</sup> with a sandwich structure of GP/PANI-G/GP (see details in the Experimental Section, Figure 4a). SEM (Figure 4b; Figure S12, Supporting Information), transmission electron microscopy (TEM) (Figure 4c,d), and Raman spectra (Figure S13, Supporting Information) exhibited 2D nanosheet morphology of mesoporous PANI strongly coupled on graphene.<sup>[47]</sup> Apparently, it can be seen that the resulting single device exhibited pronounced redox response, suggestive of a strong pseudocapacitive effect from PANI-G (Figure 4f).<sup>[5,47]</sup> Further, the resulting hybrid MSs disclosed substantially enhanced areal capacitance of  $7.6 \text{ mF cm}^{-2}$  at  $2 \text{ mV s}^{-1}$  (Figure S14, Supporting Information), much higher than that of GP-MSs ( $4.9 \text{ mF cm}^{-2}$  at  $2 \text{ mV s}^{-1}$ ). More importantly, the successful integration and performance uniformity of GP/PANI-G/GP-LTMSs from four serially connected GP/PANI-G/GP-MSs were further evidenced by both CV curves and GCD profiles (Figure 4f,g; Figure S15, Supporting Information), exhibiting a stable voltage increase from 0.8 V for GP/PANI-G/GP-MSs to 3.2 V for GP/PANI-G/GP-LTMSs. Meanwhile, GP/PANI-G/GP-MSs displayed an impressive stability, about 80.9% capacitance retention after 5000 cycles (Figure S14, Supporting Information). Therefore, these pseudocapacitive LTMSs hold great promise as a competitive high-capacitance power source for integrated electronics.

To highlight the availability of our approach, we further constructed asymmetric LTMSs (denoted as EG/MP-LTMSs) based on the printed  $\text{MnO}_2$  nanosheets/PH1000 (MP) film as

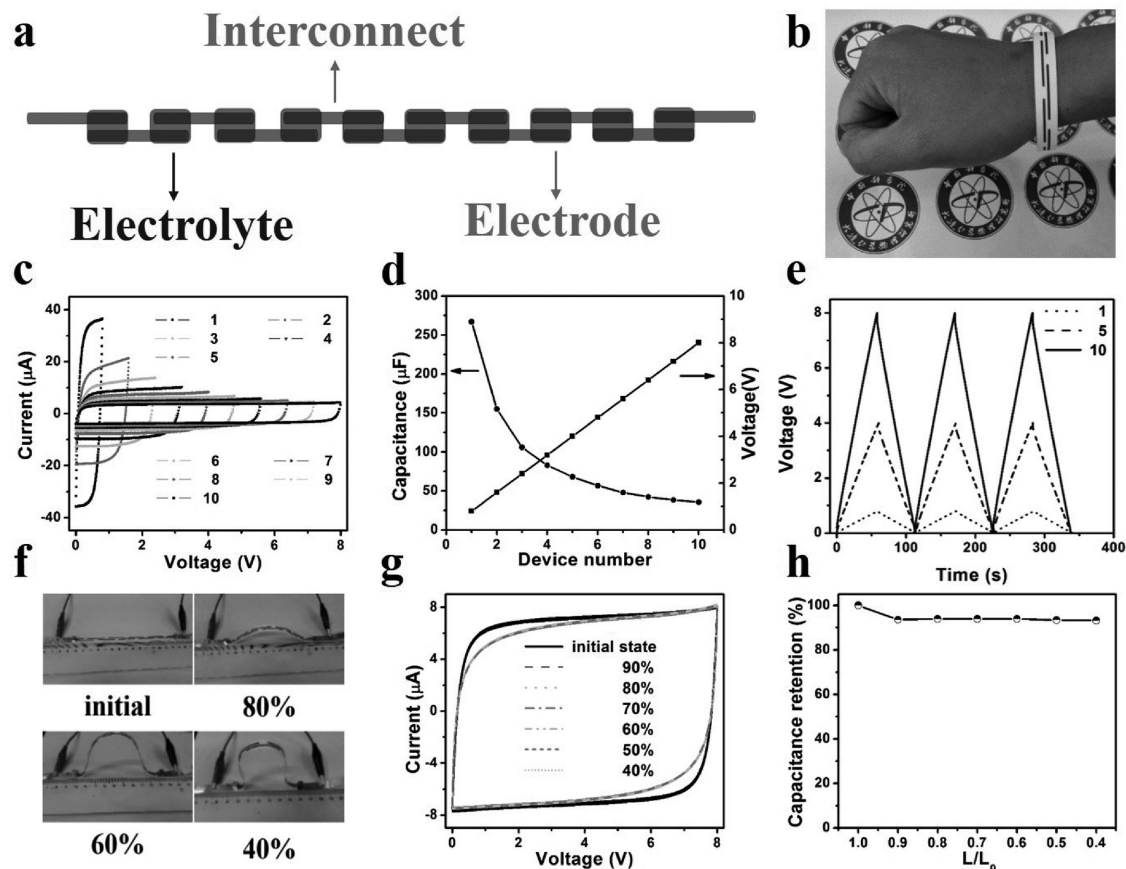


**Figure 3.** Electrochemical performance of GP-LTMSs. a) Schematic of all-solid-state GP-LTMSs connected ten GP-MSs in series. b) Photograph of GP-LTMSs encircling the wrist with 10 serially connected GP-MSs. c) CV curves of GP-LTMSs with the increasing number of serial GP-MSs, obtained at a scan rate of  $100 \text{ mV s}^{-1}$ . d) Plots of voltage output and capacitance versus serial device number. e) GCD profiles of GP-LTMSs (1, 5, 10 serially connected GP-MSs), measured at a current density of  $0.05 \text{ mA cm}^{-2}$ . f) Photograph of GP-LTMSs connected 10 GP-MSs in different bending states. g) The corresponding CV curves of GP-LTMSs measured under different bending states at  $200 \text{ mV s}^{-1}$ . h) Capacitance retention of GP-LTMSs tested under different bending states.

positive electrode and EG film as negative electrode on nylon membrane, using LiCl/PVA gel electrolyte (Figure 5). Figure 5a shows a scheme illustrating the fabrication and self-integration of asymmetric LTMSs connected three devices in series. With assistance of shape-tailored customized masks, we first spray-coated thin EG linear patterns as both interconnects and current collectors, and then deposited MP layer as positive electrodes on one side of mask, and EG layer as negative electrodes on another side of mask, respectively, on the top surface of thin EG layers (see details in the Experimental Section). TEM images (Figure 5b; Figure S16, Supporting Information) and X-ray diffraction (XRD) pattern (Figure S17, Supporting Information) of the  $\text{MnO}_2$  nanosheets, produced as described previously,<sup>[54]</sup> revealed the successful fabrication of high-quality and single-layer  $\text{MnO}_2$  nanosheets. First, we carried out electrochemical measurement of EG and MP electrodes at  $1 \text{ M LiCl}$  solution in three-electrode system to guarantee the good match of areal capacitance of EG and MP electrodes (Figure S18, Supporting Information). By applying this strategy, we found that the voltage of one asymmetric EG//MP-MS device was readily increased to  $1.8 \text{ V}$ , as evidenced by CV and GCD measurements (Figure S19, Supporting Information). Very importantly, the tailored voltage of asym-

metric EG//MP-LTMSs, serially connected three EG//MP-MSs, was stably extended to  $5.4 \text{ V}$ , triple voltage output of the single cell, demonstrating the applicability of our advanced device configuration (Figure 5f,g; Figure S20, Supporting Information). Moreover, EG//MP-LTMSs could readily powered a light emitting diode (LED) (Figure 5e), suggestive of the enormous potential of LTMSs as a microscale power source.

To further increase the energy density, we have adopted the same printable strategy to fabricate ionic-liquid-based planar MSs (denoted as EG-MSs-IL) based on pure EG films, tested with a cell voltage of  $4.0 \text{ V}$  in 1-ethyl-3-methylimidazolium tetrafluoroborate ( $\text{EMIMBF}_4$ ), as shown in Figure S21a in the Supporting Information. The Ragone plot compared volumetric energy density and power density of our GP-MSs, GP/PANI-G/GP-MSs, asymmetric EG//MP-MSs, and EG-MSs-IL with commercially available energy storage systems (Figures S21 and S22, Supporting Information). Our EG-MSs-IL offered a maximum volumetric energy density of  $19.6 \text{ mWh cm}^{-3}$ , which is much higher than GP-MSs ( $1.4 \text{ mWh cm}^{-3}$ ), GP/PANI-G/GP-MSs ( $3.1 \text{ mWh cm}^{-3}$ ), EG//MP-MSs ( $6.6 \text{ mWh cm}^{-3}$ ), activated carbon supercapacitors ( $2.75 \text{ V}/44 \text{ mF}$ ), electrolytic capacitors ( $3 \text{ V}/300 \text{ }\mu\text{F}$ ), and most reported graphene-based

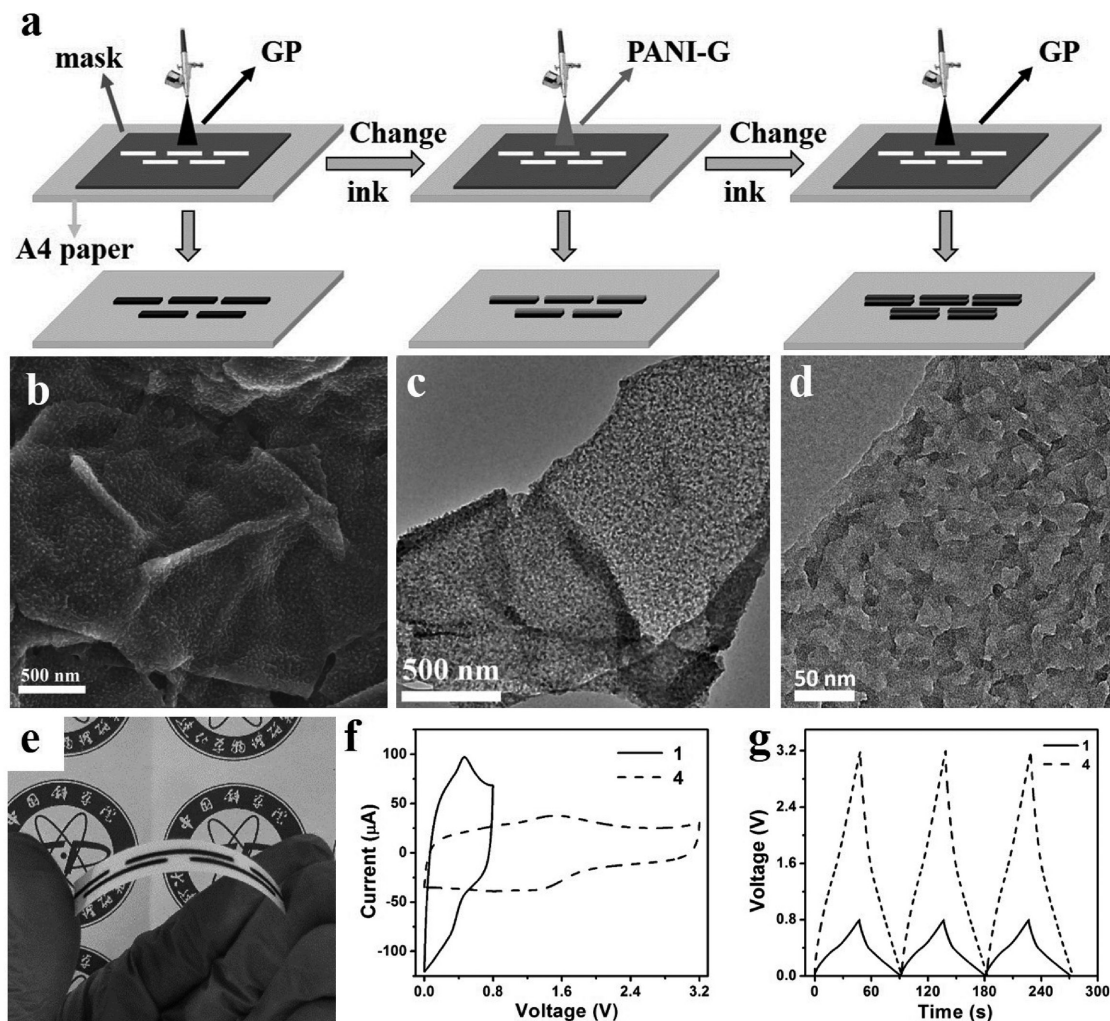


**Figure 4.** Device fabrication, characterization, and electrochemical performance of GP/PANI-G/GP-LTMSs. a) Schematic fabrication of LTMSs based on GP/PANI-G/GP film. b) SEM image of PANI-G. c) Low-magnification and d) high-magnification TEM images of PANI-G. e) Photograph of GP/PANI-G/GP-LTMSs under bending state. f) CV curves obtained at a scan rate of  $50 \text{ mV s}^{-1}$  and g) GCD profiles measured at a current density of  $0.3 \text{ mA cm}^{-2}$  of GP/PANI-G/GP-LTMSs (4 serial MSs) and GP/PANI-G/GP-MSs.

supercapacitors (Table S3, Supporting Information). Furthermore, GP-MSs possessed a maximum power density of  $2.8 \text{ W cm}^{-3}$ , exceeding activated carbon supercapacitors ( $1 \text{ W cm}^{-3}$ ), and comparable to those state-of-the-art graphene-based supercapacitors (Table S3, Supporting Information).

Our GP-LTMSs, GP/PANI-G/GP-LTMSs, and EG//MP-LTMSs all exhibited excellent electrochemical performances. The major reason was attributed to the elaborated design of high-conductive printed parallel electrodes combining the outstanding intrinsic properties (e.g., high conductivity and high capacitance) of 2D nanosheets and high electrical conductivity of PH1000.<sup>[8,13]</sup> In addition, three kinds of ultrathin 2D nanosheets, including EG, PANI-G, and  $\text{MnO}_2$  nanosheets were selected as electrode materials for planar supercapacitors, in which the electrolyte ions could shuttle easily along the plane of 2D nanosheets, minimizing the resistance of ionic diffusion.<sup>[25,45]</sup> These results further underscored the appealing features of our LTMSs capable of high-voltage output, tailored capacitance, versatile device configuration, excellent flexibility,

and self-integration without the use of metal-based interconnects and current collectors.

In summary, we have demonstrated a universal and scalable technology to engineer a novel class of graphene-based LTMSs, with high-voltage output, metal-free current collectors and interconnects, tailored capacitance, desirable device planar configuration, outstanding flexibility, excellent integration, and applicability, for on-chip energy storage. In comparison with previously reported MSs,<sup>[29,33]</sup> there are several specific novelty and advantages of our LTMSs. First, a class of new-concept planar LTMSs with superior serial integration, without requirement of metal-based current collectors and interconnects, was demonstrated, which is a big advanced device geometry innovation in both integration and linear shape. Second, our strategy was a cheap, efficient, and simplified technique for the facile production of linear tandem structure, in which the deposition, patterning, and serial integration of linear tandem electrodes were achieved in one step. Third, our LTMSs are very promising to be directly compatible with the printed electronics integrated

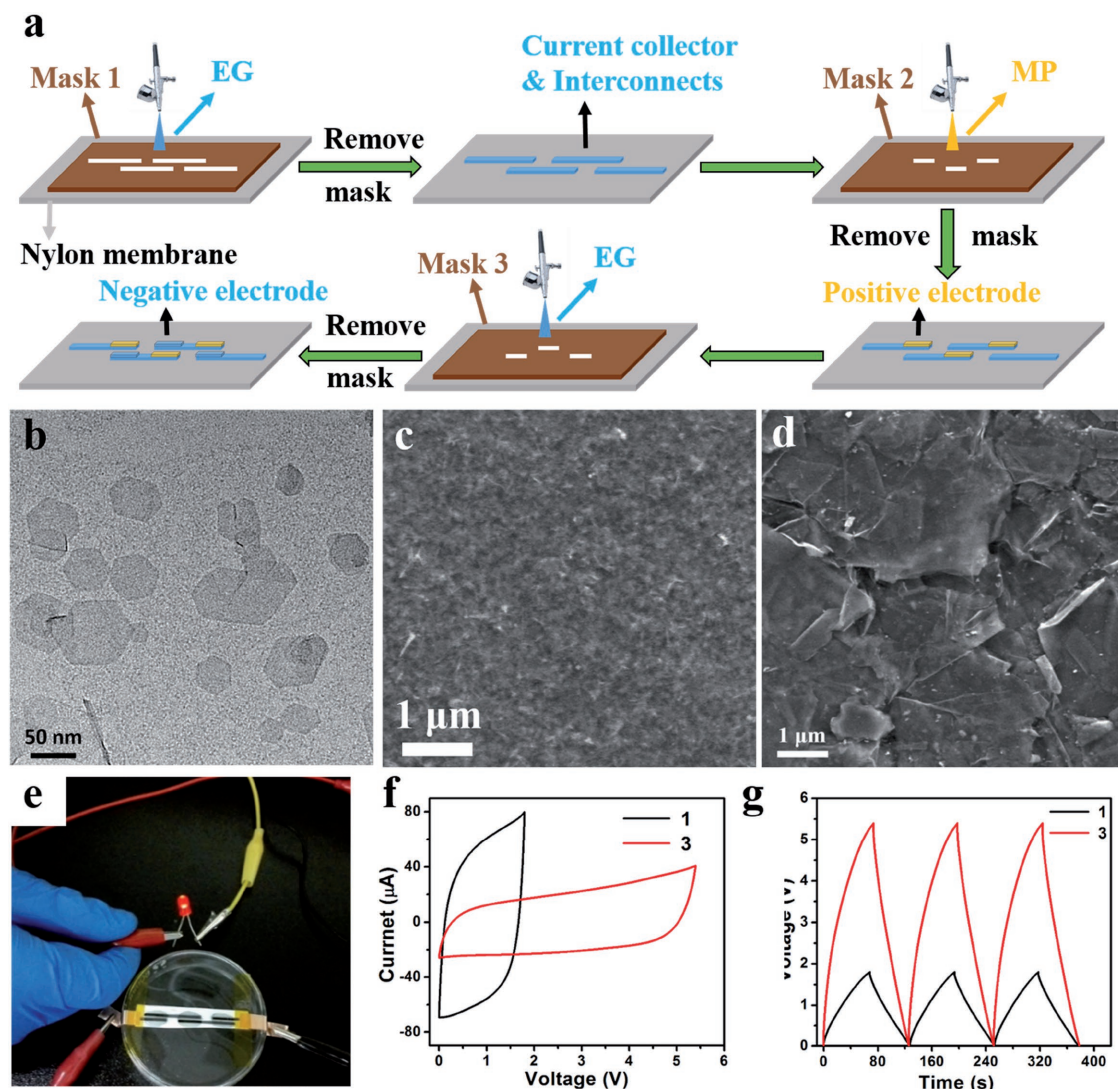


**Figure 5.** Device fabrication, characterization, and electrochemical performance of asymmetric EG//MP-LTMSs based on EG film as negative electrodes and MP film as positive electrodes. a) A scheme illustrating the fabrication and self-integration of asymmetric EG//MP-LTMSs serially connected three asymmetric MSs. b) TEM image of  $\text{MnO}_2$  nanosheets. c,d) Top-view SEM images of c) MP positive electrode and d) EG negative electrode in asymmetric EG//MP-MSs. e) Photograph of asymmetric EG//MP-LTMSs powering a LED. f) CV curves obtained at a scan rate of  $100 \text{ mV s}^{-1}$  and g) GCD profiles measured at a current density of  $0.2 \text{ mA cm}^{-2}$  of asymmetric EG//MP-LTMSs (3 EG//MP-MSs).

on single substrate, and our versatile printable technique can be directly extended to inkjet printing,<sup>[55]</sup> 3D printing,<sup>[56]</sup> screen printing,<sup>[17]</sup> and roll-to-roll process<sup>[57]</sup> for mass production of LTMSs. Last but not least, our LTMSs with diverse 2D materials, symmetric and asymmetric constructions were fabricated successfully on various substrates, indicating their outstanding applicability. Especially, the success of asymmetric linear tandem supercapacitors paved a way to build similar construction for other planar energy storage systems, e.g., batteries. All of these could not be achieved with conventional technologies.<sup>[29,33]</sup> Sufficient combination of printable technique and 2D nanosheets greatly simplify the fabrication and integration of LTMSs for modular power source units to meet the stringent requirement of electronics in form factors of performance and functionalities. We believe that our demonstration of LTMSs will offer the opportunities to construct new-concept planar

self-power integrated system composed of high-voltage tandem energy storage devices and printed electronics on a single substrate.

## Experimental Section

**Fabrication of GP-MSs and GP-LTMSs:** GP ink was obtained through the addition of 1 mL PH1000 (poly(3,4-ethylenedioxythiophene)-poly(styrenesulfonate), solid content of 1–1.3 wt%, Heraeus Clevios GmbH) aqueous solution into 20 mL supernatant of  $0.6 \text{ mg mL}^{-1}$  EG/IPA by sonication for 30 min. GP-MSs with different loading ink volume were fabricated by spray-coating 0.5, 1.0, 1.5, 2.0, 2.5 mL GP ink onto A4 paper with the assistance of parallel linear mask (1.5 cm length and 0.1 cm width of single electrode, 0.1 cm interspace). GP-LTMSs were fabricated by spray-coating 10 mL GP ink onto A4 paper with the assistance of an inconsecutively parallel linear customized mask

(1.0 cm length and 0.1 cm width of single electrode, 0.1 cm interspace between two electrodes, and 0.5 cm length of interconnect, total length of 14.5 cm). Afterward, H<sub>2</sub>SO<sub>4</sub>/PVA gel electrolyte was carefully drop-casted on the surface of linear electrodes and solidified overnight. Note that the interconnects of GP-LTMSs were not covered by gel electrolyte.

**Fabrication of GP/PANI-G/GP-MSs and GP/PANI-G/GP-LTMSs:** PANI-G ink with a concentration of 0.5 mg mL<sup>-1</sup> was obtained by adding PANI-G into 9 mL IPA by sonication for 1 h. GP/PANI-G/GP-MSs were obtained through step-by-step spray coating of 0.5 mL GP ink, 0.5 mL PANI-G ink, and 0.5 mL GP ink onto A4 paper with the assistance of the same customized patterned mask. GP/PANI-G/GP-LTMSs consisting of four GP/PANI-G/GP-MSs were obtained through the same step-by-step spray coating of 1.5 mL GP ink, 1.5 mL PANI-G ink, and 1.5 mL GP ink onto A4 paper, with the assistance of the similar inconsecutively parallel linear mask (1.0 cm length and 0.1 cm width of single electrode, 0.1 cm interspace between two electrodes, 0.5 cm length of interconnect, and total length of GP-LTMSs of 5.5 cm). Afterward, H<sub>2</sub>SO<sub>4</sub>/PVA gel electrolyte was carefully drop-casted onto the electrodes and solidified overnight.

**Fabrication of Asymmetric EG//MP-MSs and EG//MP-LTMSs:** MP ink was prepared by adding 0.4 mL 2.7 mg mL<sup>-1</sup> MnO<sub>2</sub> nanosheets and 0.1 mL PH1000 into a mixed solution (5.5 mL deionized water and 6 mL methanol) by sonication for 30 min. The single asymmetric EG//MP-MSs were fabricated by spray-coating 1 mL 0.5 mg mL<sup>-1</sup> EG/IPA ink onto nylon membrane as current collectors first, and then spray-coating 0.9 mL MP ink as positive electrode with the customized mask (only positive electrode was exposed) and 0.5 mL EG/IPA ink as negative electrode with the customized mask (only negative electrode was exposed), respectively. The serially connected asymmetric EG//MP-LTMSs consisting of three EG//MP-MSs were manufactured through spray-coating 2.4 mL 0.5 mg mL<sup>-1</sup> EG/IPA ink as current collectors first with a customized mask (1.0 cm length and 0.1 cm width of single electrode, 0.1 cm interspace between two electrodes, 0.5 cm length of interconnect, and total length of 4 cm), then spray-coating 0.5 mL MP ink as positive electrodes with the mask 1 (only positive electrode was exposed) and 0.3 mL EG/IPA ink as negative electrodes with the mask 2 (only negative electrode was exposed), respectively. Afterward, the nylon membrane was pressed with a power compressing machine (769YP-15A) under a pressure of 20 MPa. Finally, LiCl/PVA gel electrolyte was carefully drop-casted onto the electrodes and solidified overnight.

**Materials Characterization:** Materials characterization was conducted by SEM (JEOL JSM-7800F), high resolution TEM (HRTEM) (JEM-2100), AFM (Veeco nanoscope multimode II-D), Raman spectroscopy (LabRAM HR 800 Raman spectrometer, 632 nm), XRD patterns (X'pert Pro).

**Electrochemical Measurement:** The electrochemical performance of the supercapacitors was evaluated by CV measurements at different scan rates, GCD profiles conducted at different current densities, and electrochemical impedance spectroscopy recorded in the frequency range from 0.01 Hz to 100 kHz with a 5 mV ac amplitude, using an electrochemical workstation (CHI 760E).

**Calculation:** The capacitance values were calculated from the discharge CV curves according to the following formula (1)

$$C = \frac{1}{\nu(V_f - V_i)} \int_{V_i}^{V_f} I(V) dV \quad (1)$$

where  $\nu$  is the scan rate (V s<sup>-1</sup>),  $V_f$  and  $V_i$  are the integration potential limits of the voltammetric curve, and  $I(V)$  is the voltammetric discharge current (A).

Specific capacitance of device was calculated based on the area and volume of the device according to the following formulas (2) and (3)

$$C_{\text{device}}^{\text{areal}} = C/A_{\text{device}} \quad (2)$$

$$C_{\text{device}}^{\text{vol}} = C/V_{\text{device}} \quad (3)$$

where  $C_{\text{device}}^{\text{areal}}$  (F cm<sup>-2</sup>) and  $C_{\text{device}}^{\text{vol}}$  (F cm<sup>-3</sup>) refer to the areal capacitance and volumetric capacitance of device, respectively.  $A_{\text{device}}$  and  $V_{\text{device}}$  are

the total area and volume of the positive and negative electrodes in device, respectively.

The volumetric energy density of the device was obtained from the following formula (4)

$$E = \frac{1}{2} \times C_{\text{device}}^{\text{vol}} \times \frac{(\Delta V)^2}{3600} \quad (4)$$

where  $E$  is the energy density (Wh cm<sup>-3</sup>),  $C_{\text{device}}^{\text{vol}}$  is the volumetric capacitance obtained from formula (3), and  $\Delta V$  is the discharge voltage range (V).

The power density of the device was calculated from the following formula (5)

$$P = \frac{E}{\Delta t} \times 3600 \quad (5)$$

where  $P$  is the power density (W cm<sup>-3</sup>),  $E$  is the volumetric energy density obtained from formula (4), and  $\Delta t$  is the discharge time (s).

## Supporting Information

Supporting Information is available from the Wiley Online Library or from the author.

## Acknowledgements

This work was financially supported by the National Natural Science Foundation of China (Grant 51572259), Ministry of Science and Technology of China (Grants 2016YBF0100100, 2016YFA0200200), Recruitment Program of Global Expert (1000 Talent Plan), Natural Science Foundation of Liaoning Province (Grant 201602737), DICP (Grant Y5610121T3), and Exploratory Research Projects of Shaanxi Yanchang Petroleum (Group) CO., LTD & DICP.

## Conflict of Interest

The authors declare no conflict of interest.

## Keywords

2D nanosheets, graphene, high voltage, metal-free current collectors, micro-supercapacitors

Received: May 31, 2017

Revised: September 10, 2017

Published online: October 13, 2017

- [1] B. D. Gates, *Science* **2009**, *323*, 1566.
- [2] W. Liu, M. S. Song, B. Kong, Y. Cui, *Adv. Mater.* **2017**, *29*, 1603436.
- [3] L. Wen, F. Li, H.-M. Cheng, *Adv. Mater.* **2016**, *28*, 4306.
- [4] H. Wu, Y. Huang, F. Xu, Y. Duan, Z. Yin, *Adv. Mater.* **2016**, *28*, 9881.
- [5] L. Yuan, X. Xiao, T. Ding, J. Zhong, X. Zhang, Y. Shen, B. Hu, Y. Huang, J. Zhou, Z. L. Wang, *Angew. Chem., Int. Ed.* **2012**, *51*, 4934.
- [6] Y. Yue, Z. Yang, N. Liu, W. Liu, H. Zhang, Y. Ma, C. Yang, J. Su, L. Li, F. Long, Z. Zou, Y. Gao, *ACS Nano* **2016**, *10*, 11249.
- [7] M. Kaempgen, C. K. Chan, J. Ma, Y. Cui, G. Gruner, *Nano Lett.* **2009**, *9*, 1872.
- [8] Z. S. Wu, Z. Liu, K. Parvez, X. Feng, K. Müllen, *Adv. Mater.* **2015**, *27*, 3669.

- [9] K.-H. Choi, J. Yoo, C. K. Lee, S.-Y. Lee, *Energy Environ. Sci.* **2016**, *9*, 2812.
- [10] S. Zheng, X. Tang, Z. S. Wu, Y. Z. Tan, S. Wang, C. Sun, H. M. Cheng, X. Bao, *ACS Nano* **2017**, *11*, 2171.
- [11] J. R. Miller, *Science* **2012**, 335, 1312.
- [12] S. Lehtimäki, M. Li, J. Salomaa, J. Pörhönen, A. Kalanti, S. Tuukkanen, P. Heljo, K. Halonen, D. Lupo, *Int. J. Electr. Power Energy Syst.* **2014**, *58*, 42.
- [13] Z. Liu, Z. S. Wu, S. Yang, R. Dong, X. Feng, K. Müllen, *Adv. Mater.* **2016**, *28*, 2217.
- [14] X. Ji, P. M. Hallam, S. M. Houssein, R. Kadara, L. Lang, C. E. Banks, *RSC Adv.* **2012**, *2*, 1508.
- [15] X. Zhao, C. Johnston, A. Crossley, P. S. Grant, *J. Mater. Chem.* **2010**, *20*, 7637.
- [16] P. Chen, H. Chen, J. Qiu, C. Zhou, *Nano Res.* **2010**, *3*, 594.
- [17] Y. Xu, M. G. Schwab, A. J. Strudwick, I. Hennig, X. Feng, Z. Wu, K. Müllen, *Adv. Energy Mater.* **2013**, *3*, 1035.
- [18] E. H. Kil, K. H. Choi, H. J. Ha, S. Xu, J. A. Rogers, M. R. Kim, Y. G. Lee, K. M. Kim, K. Y. Cho, S. Y. Lee, *Adv. Mater.* **2013**, *25*, 1395.
- [19] M. Koo, K. I. Park, S. H. Lee, M. Suh, D. Y. Jeon, J. W. Choi, K. Kang, K. J. Lee, *Nano Lett.* **2012**, *12*, 4810.
- [20] Y. Xu, I. Hennig, D. Freyberg, A. J. Strudwick, M. G. Schwab, T. Weitz, K. C.-P. Cha, *J. Power Sources* **2014**, *248*, 483.
- [21] J. Yeo, G. Kim, S. Hong, M. S. Kim, D. Kim, J. Lee, H. B. Lee, J. Kwon, Y. D. Suh, H. W. Kang, H. J. Sung, J.-H. Choi, W.-H. Hong, J. M. Ko, S.-H. Lee, S.-H. Choa, S. H. Ko, *J. Power Sources* **2014**, *246*, 562.
- [22] C. Zhu, T. Liu, F. Qian, T. Y. Han, E. B. Duoss, J. D. Kuntz, C. M. Spadaccini, M. A. Worsley, Y. Li, *Nano Lett.* **2016**, *16*, 3448.
- [23] X. Yang, C. Cheng, Y. Wang, L. Qiu, D. Li, *Science* **2013**, *341*, 534.
- [24] M. F. El-Kady, V. Strong, S. Dubin, R. B. Kaner, *Science* **2012**, 335, 1326.
- [25] J. J. Yoo, K. Balakrishnan, J. Huang, V. Meunier, B. G. Sumpter, A. Srivastava, M. Conway, A. L. Reddy, J. Yu, R. Vajtai, P. M. Ajayan, *Nano Lett.* **2011**, *11*, 1423.
- [26] K. Wang, W. Zou, B. Quan, A. Yu, H. Wu, P. Jiang, Z. Wei, *Adv. Energy Mater.* **2011**, *1*, 1068.
- [27] Z. S. Wu, X. Feng, H. M. Cheng, *Natl. Sci. Rev.* **2013**, *1*, 277.
- [28] J. Liu, *Nat. Nanotechnol.* **2014**, *9*, 739.
- [29] C. Meng, J. Maeng, S. W. M. John, P. P. Irazoqui, *Adv. Energy Mater.* **2014**, *4*, 1301269.
- [30] N. A. Kyeremateng, T. Brousse, D. Pech, *Nat. Nanotechnol.* **2017**, *12*, 7.
- [31] M. Beidaghi, Y. Gogotsi, *Energy Environ. Sci.* **2014**, *7*, 867.
- [32] W. Gao, N. Singh, L. Song, Z. Liu, A. L. Reddy, L. Ci, R. Vajtai, Q. Zhang, B. Wei, P. M. Ajayan, *Nat. Nanotechnol.* **2011**, *6*, 496.
- [33] M. F. El-Kady, R. B. Kaner, *Nat. Commun.* **2013**, *4*, 1475.
- [34] D. Qi, Y. Liu, Z. Liu, L. Zhang, X. Chen, *Adv. Mater.* **2017**, *29*, 1602802.
- [35] Z. S. Wu, K. Parvez, X. Feng, K. Müllen, *Nat. Commun.* **2013**, *4*, 2487.
- [36] Z. Niu, L. Zhang, L. Liu, B. Zhu, H. Dong, X. Chen, *Adv. Mater.* **2013**, *25*, 4035.
- [37] J. Lin, Z. Peng, Y. Liu, F. Ruiz-Zepeda, R. Ye, E. L. Samuel, M. J. Yacaman, B. I. Yakobson, J. M. Tour, *Nat. Commun.* **2014**, *5*, 5714.
- [38] Z.-K. Wu, Z. Lin, L. Li, B. Song, K.-s. Moon, S.-L. Bai, C.-P. Wong, *Nano Energy* **2014**, *10*, 222.
- [39] J. Chang, S. Adhikari, T. H. Lee, B. Li, F. Yao, D. T. Pham, V. T. Le, Y. H. Lee, *Adv. Energy Mater.* **2015**, *5*, 1500003.
- [40] Z. S. Wu, Y. Z. Tan, S. Zheng, S. Wang, K. Parvez, J. Qin, X. Shi, C. Sun, X. Bao, X. Feng, K. Müllen, *J. Am. Chem. Soc.* **2017**, *139*, 4506.
- [41] Y.-Y. Peng, B. Akuzum, N. Kurra, M.-Q. Zhao, M. Alhabeab, B. Anasori, E. C. Kumbur, H. N. Alshareef, M.-D. Ger, Y. Gogotsi, *Energy Environ. Sci.* **2016**, *9*, 2847.
- [42] N. Kurra, B. Ahmed, Y. Gogotsi, H. N. Alshareef, *Adv. Energy Mater.* **2016**, *6*, 1601372.
- [43] H. Li, Y. Hou, F. Wang, M. R. Lohe, X. Zhuang, L. Niu, X. Feng, *Adv. Energy Mater.* **2017**, *7*, 1601847.
- [44] J. Feng, X. Sun, C. Wu, L. Peng, C. Lin, S. Hu, J. Yang, Y. Xie, *J. Am. Chem. Soc.* **2011**, *133*, 17832.
- [45] Z. S. Wu, Y. Zheng, S. Zheng, S. Wang, C. Sun, K. Parvez, T. Ikeda, X. Bao, K. Müllen, X. Feng, *Adv. Mater.* **2017**, *29*, 1602960.
- [46] S. Liu, P. Gordiichuk, Z. S. Wu, Z. Liu, W. Wei, M. Wagner, N. Mohamed-Noriega, D. Wu, Y. Mai, A. Herrmann, K. Müllen, X. Feng, *Nat. Commun.* **2015**, *6*, 8817.
- [47] Z. S. Wu, K. Parvez, S. Li, S. Yang, Z. Liu, S. Liu, X. Feng, K. Müllen, *Adv. Mater.* **2015**, *27*, 4054.
- [48] S. Wang, S. H. Zheng, Z. S. Wu, C. L. Sun, *Sci. Sin. Chim.* **2016**, *46*, 732.
- [49] K. Parvez, R. Li, S. R. Puniredd, Y. Hernandez, F. Hinkel, S. Wang, X. Feng, K. Müllen, *ACS Nano* **2013**, *7*, 3598.
- [50] K. Parvez, Z. S. Wu, R. Li, X. Liu, R. Graf, X. Feng, K. Müllen, *J. Am. Chem. Soc.* **2014**, *136*, 6083.
- [51] J. Lin, C. Zhang, Z. Yan, Y. Zhu, Z. Peng, R. H. Hauge, D. Natelson, J. M. Tour, *Nano Lett.* **2013**, *13*, 72.
- [52] K. Sheng, Y. Sun, C. Li, W. Yuan, G. Shi, *Sci. Rep.* **2012**, *2*, 247.
- [53] D. Pech, M. Brunet, P.-L. Taberna, P. Simon, N. Fabre, F. Mesnilgrentre, V. Conédéra, H. Durou, *J. Power Sources* **2010**, *195*, 1266.
- [54] S. Rong, P. Zhang, Y. Yang, L. Zhu, J. Wang, F. Liu, *ACS Catal.* **2017**, *7*, 1057.
- [55] J. Li, F. Ye, S. Vaziri, M. Muhammed, M. C. Lemme, M. Ostling, *Adv. Mater.* **2013**, *25*, 3985.
- [56] K. Sun, T. S. Wei, B. Y. Ahn, J. Y. Seo, S. J. Dillon, J. A. Lewis, *Adv. Mater.* **2013**, *25*, 4539.
- [57] S. H. Ahn, L. J. Guo, *Adv. Mater.* **2008**, *20*, 2044.